GPPS-2018-0038

Modelling the Rubbing Process in Labyrinth Seals

Oliver Munz, Corina Schwitzke, Hans-Jörg Bauer
Institute of Thermal Turbomachinery
oliver.munz@kit.edu
Karlsruhe, Germany

Sarah Welzenbach, Tim Fischer
Institute of Materials Science and Mechanics of Materials
Garching, Germany

Sonun Ulan kyzy
Metals and Alloys
Bayreuth, Germany

ABSTRACT

To understand the complex rubbing process between labyrinth seal fins and honeycomb liners, experimental investigations are considered for an idealized contact between a metal sheet, representing the honeycomb part, and a rotating seal fin. Modifications of our test rig allow to measure the resulting rub forces, temperatures and wear of the seal fin and metal sheet for a wide range of circumferential velocities and incursion rates. The rotor material is Inconel 718, and the metal sheets consist of the nickel-based super-alloys Hastelloy X and Haynes 214. To define appropriate boundary conditions for the experiment, a one-dimensional numerical model is introduced. It takes into account kinematic contact conditions, friction, heat conduction, and abrasive and plastic wear. The use of analytical relations and parallel computing enables a time-efficient computation of multiple scenarios. Therefore, it is possible to identify the effect of variations and uncertainties of the input parameters on the results and derive an optimized test plan.

INTRODUCTION

The increasing responsibility for environmentally beneficial and sustainable mobility in today's aircraft engine development leads to the main goal of increasing efficiency and reducing fuel consumption [6]. Core engines, therefore, are operated at a higher turbine inlet temperature and an increasing pressure ratio. The increasing power density results in a substantial potential by significantly increasing component efficiency and thus overall efficiency through cost-effective developments.

Reducing the clearance in the flow paths and secondary air system is an effective method to minimize the airflow leakage [3, 17]. The most frequently used sealing system is the labyrinth seal [5]. In addition to reducing the leakage mass flow, the seal has to tolerate rubbing events caused by thermal and mechanical expansion of rotor and casing or manoeuvre loads. Abradable liner materials are used to protect the rotor by providing a fast and controlled wear of the stator.

To understand the complex rubbing process between labyrinth seal fins and abradable liners, which may cause detrimental heat input into the rotating structure and lead to severe damages, experimental and numerical investigations in the literature are considered. The research can be divided into investigations on rubbing between a rotating seal and static casing, and blade rubs against the stator or a vane. A comprehensive review about experimental and numerical studies regarding blade-rubbing can be found in Ma et al. [12] and will not be discussed further in this context.

Bill and Ludwig [2] point out the difference between abradable seal materials such as porous materials, low shear strength materials and honeycomb structures. Observations from experiments with Hastelloy-X honeycombs show that braze nodes at the interface between two metal foils can be critical points because their thickness is up to two to three times higher. Optical examination after the rub tests shows hot spots both on the honeycomb liner and the rotor.

Experimental investigations by Ghasripoor et al. [8] show that the thermal conductivity and aspect ratio of strip seals mainly influence wear. The mechanisms for high-speed wear are melting and mushrooming. Materials with low thermal conductivity exhibit significantly higher wear.

Mutasim et al. [13] observed smooth cutting edges, smearing and material transfer in the investigation of several sprayed thermal coatings using a labyrinth test rig.

The test rig presented in Rathmann et al. [16] enables both tests with blades as well as labyrinth seals. The results were validated with observations from real engines, but no data for honeycomb shroud interactions was presented.

Delebarre et al. [7] developed a high-speed test rig to study the wear behaviour between an Al-Si 6% coating and a stainless-steel labyrinth seal for high incursion rates of up to 9.41 mm/s and low labyrinth seal speeds of 17 m/s. The tribological contact was studied by use of high-speed imaging.

Herrmann et al. [11] obtained experimental data from a wear test rig to calibrate and validate a numerical finite element analysis focusing on plastic wear phenomena. With

this approach, it was possible to study the wear behaviour of three labyrinth seal configurations and observe a considerable gain in performance by the use of seal strips.

Zhang et al. [19] measured the forces and the dynamic impact response for a shrouded blade with labyrinth tips and a honeycomb sample. The results show a strong dependence on the incursion rate. Under the effect of high temperatures, smearing and adhesive material transfer could be observed. They also identified the maximum value of the rubbing force as a predictor for the degree of damage.

The rubbing process is currently the subject of several studies. Nevertheless, the demand for experimental and numerical investigations of the contact between the sealing fin and the honeycomb liner is not sufficiently covered.

Considering the geometry of the honeycomb in Figure 1 a contact with the seal fin results in complex contact geometries. In order to understand the system and increase the physical understanding, Pychynski et al. [15] studied the contact between a labyrinth seal fin and a single metal foil for a steel to steel material combination. The current study aims to determine the effect of different material combinations.
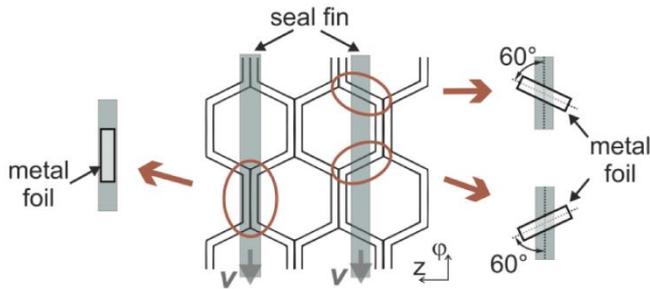

Figure 1 Schematic drawing of a honeycomb liner, and rub positions of a labyrinth seal fin [15]

EXPERIMENTAL SETUP

The test rig set up by Pychynski et al. [15] is depicted in Figure 2 and will be used to study the friction behaviour of an Inconel 718 rotor rubbing against Hastelloy X and Haynes 214 metal foils. Therefore, the test rig is modified to allow for higher circumferential velocities and higher incursion rates. Three labyrinth seal fins were manufactured on the rotor circumference providing both inclined and perpendicular seal fin geometries. The maximum relative velocity of the rotor surface results for the rotor diameter of 360 mm, powered by an electric motor, to 200 m/s. A traversing system is able to provide an incursion rate of 1.5 mm/s. The thickness of the rest metal foils will be 0.3 to 0.6 mm. A special foil holder is mounted to the cross head of the traversing system which is driven by a linear stepper motor. The foil holder allows three orientations for the metal foils, depicted in Figure 1.

To measure the resulting coefficient of friction, a three-component piezo electric force meter is installed at the mount. The axial displacement of the traversing system can be adjusted in such a way that all three seal fins can be tested. Beside the resulting friction forces, the temperatures in the contact zone are of great interest.
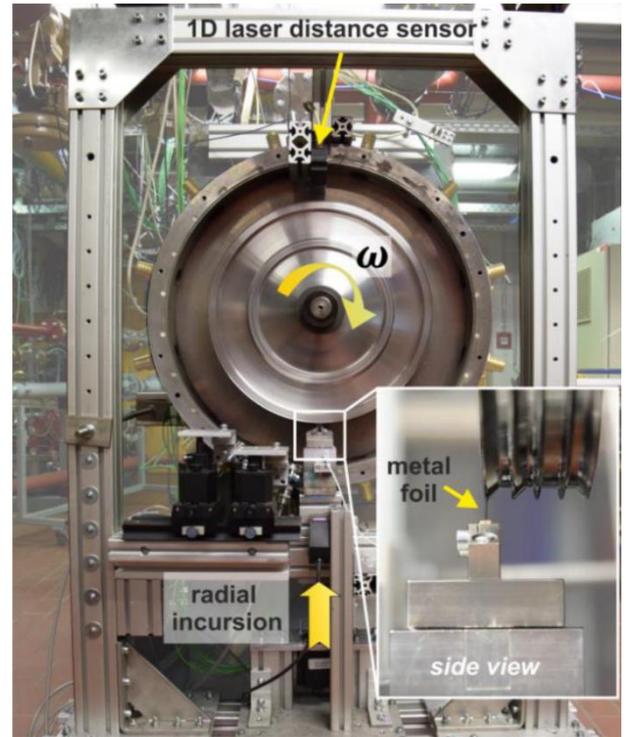
Figure 2 Axial front and side views of the rest rig [15]

To measure the temperature of the static foil, an infrared camera is used. To achieve an accurate temperature measurement, the surfaces of the metal foils are coated in order to get a homogeneous and highly emissive surface. The temperature at the seal fin tip is measured with two high-speed pyrometers using different wavelengths accounting for different temperature ranges. A torque transducer also determines the torque of the electric motor and enables calculation of the friction power.

In Figure 3, the test matrix for the varied conditions rub velocity v_r and incursion rate $\dot{s}$ is shown. In addition, the final incursion depth s_{final} is varied from 0.5 to 1.5 mm. Conducting the experiments for two seal fin geometries and varying thickness, orientation and material of the metal foil leads to a large amount of different scenarios. Therefore, an implemented model for the rubbing behaviour is used to adjust the test plan so that most relevant working points are covered and the experimental effort is reduced.
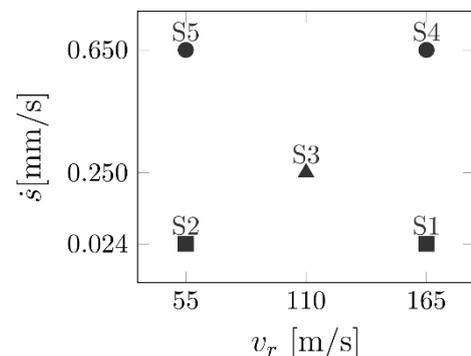
Figure 3 Test matrix with rub scenarios S1-S5

MODEL

The modelling approach was introduced by Pychynski [14] to reproduce the experimental test results and gain insights into the physical effects during a rubbing process. The use of analytical formulations and parallel computing allows for low computational costs. Fast prediction of multiple scenarios enables the use of statistical methods to identify the main input parameters.

In order to reduce the computational costs of the simulations, the rubbing process is simplified to a one-dimensional approach as shown in Figure 4. All parameters describe macroscopic quantities and the average over a rotor revolution. One of the main findings in the conducted experiments by Pychynski et al. [15] is that over a rotor revolution, the contact is only established during 15% of the time. Therefore, all discussed parameters $\bar{y}$ are averaged over a rotor revolution and based on the adjusted segment angle φ_{ec} (see Figure 4).

$$y = \frac{2\pi}{\varphi_{ec}} \bar{y} \qquad (1)$$

Boundary conditions

The applied boundary conditions are depicted in Figure 4. The seal fin tip has a diameter of 210 mm, is 4 mm high and has a width of 0.8 mm. The metal foil has a length of 20 mm and a width of 0.4 to 0.6 mm. Originally, the metal foil of the experiment has a height of 20 mm, but because it is mounted into the special metal holder, only 8 mm are taken into account in the model.

Kinematic contact

For the kinematic contact conditions, it is assumed that the foil and the seal fin are in continuous contact and the contact pressure p_c is distributed uniformly over the nominal contact area A_C. The contact pressure p_c is then a function of the real incursion s_{real}:

$$p_C = s_{real}\, k. \qquad (2)$$

The parameter k is the radial stiffness obtained by serially adding the stiffness of the metal foil and the structure as spring elements. The stiffness is calculated for the specific geometry and is pressure-dependent. The real incursion is affected by the theoretical incursion of the metal foil, following from the constant incursion velocity. Additionally, the thermal expansion and the total wear are considered.

Friction

Friction is described by Coulomb's Law of Friction resulting in a macroscopic friction force F only depending on a coefficient of friction μ and the normal load:

$$F = \mu\, p_C A_C. \qquad (3)$$

The coefficient of friction was derived from experimental test results and remains constant over the rubbing process for a given scenario (see Figure 3). Assuming a constant and uniform coefficient of friction leads to a friction heat flux $\dot{q}_{fric}$ that is only depending on the friction velocity v_r and force.

$$\dot{q}_{fric} = \mu\, p_C\, v_r \qquad (4)$$

Temperature

The temperatures in the contact zone of the rubbing process have a large influence on the contact pressure, friction and wear behaviour of the system. Moreover, for high temperatures achieved during a rubbing process in labyrinth seals, the influence of the material properties is of great significance. Therefore, a crucial part is the prediction of the resulting temperatures of the thermal contact model.

It is assumed that the friction energy is only dissipated in the contact surface. Because dissipation is a process on the microscale and depends, for example, on the microscopic plastic deformations, an intrinsic partitioning factor β_i is defined such that the resulting heat fluxes in metal foil $\dot{q}_{foil}$ and seal fin $\dot{q}_{sf}$ can be formulated as a macroscopic quantity.

$$\dot{q}_{foil} = \beta_i\, \dot{q}_{fric}, \quad \dot{q}_{sf} = (1 - \beta_i)\, \dot{q}_{fric} \qquad (5)$$
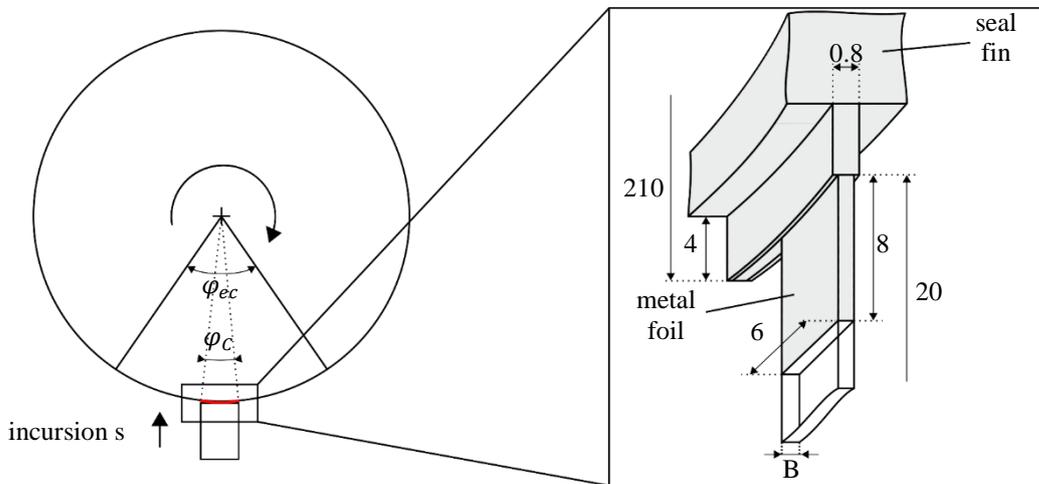

Figure 4 Contact conditions of the model approach on the left, boundary conditions on the right

Chassaing et al. [4] introduced a promising method to calculate the heat partitioning in high speed applications. Due to missing information, in this study it is assumed that the heat is partitioned evenly between the seal fin and the metal foil. The contact is defined as a perfect contact with a heat flux $\dot{q}_C$ from the metal foil to the seal fin:

$$\dot{q}_C = h_C \left(T_{C,foil} - T_{C,sf} \right) \qquad (6)$$

with the heat transfer coefficient

$$h_C = h_{C,0}\, \lambda_{eff} \left(\frac{p_c}{E(T_C)} \right)^2 \qquad (7)$$

where λ_{eff} is the effective thermal conductivity, E the Young's modulus of the softer friction partner and the parameter $h_{C,0}$. As a result of the thermal contact model, an effective heat partitioning factor can be calculated as

$$\beta_{eff} = \frac{\dot{q}_{eff,foil}}{\dot{q}_{fric}}. \qquad (8)$$

It describes the ratio of heat flux flowing in the metal foil and is a function of the temperatures of seal fin and metal foil, the area of the contact, the intrinsic heat partitioning factor, and the heat transfer coefficient.

The thermal model also takes into account the influence of a moving heat source by applying a factor to the constant heat flux over one circumference. The resulting heat fluxes in the contact are used as input parameters for numerical finite difference models to calculate the one-dimensional temperature field in metal foil and seal fin.

Wear

The results obtained by Pychynski et al. [15] for a steel-steel contact show that the wear of the seal fin can be neglected. For the metal foil, the total wear

$$w_{tot} = w_a + w_{pl} \qquad (9)$$

is a function of the abrasive wear w_a and the plastic wear w_{pl}, respectively. The abrasive wear is modelled by the Archard wear equation [1]. This idealized model describes the abrasive wear rate

$$\dot{w}_a = k_{w,a}\, p_C\, \frac{1}{E}\, v_r \qquad (10)$$

as a relation of the contact pressure p_C, the friction velocity v_r, the Young's modulus E, and the parameter $k_{w,a}$.

The plastic wear model was derived from a compression strut. To take into account the viscoplastic material behaviour at high temperatures, a time constant t_{pl} was formulated such that:

$$\dot{w}_{pl} = \left(1 - k_{w,pl}\, \frac{R_{p02}}{p_C} \right) \frac{s_{real}\, v_r}{2\,\pi\, r_{sf}} \left(1 - e^{\left(-\frac{\varphi_{ec}\, r_{sf}}{t_{pl}\, v_r} \right)} \right) \qquad (11)$$

for $p_C > k_{w,pl}\, R_{p02}$ with the scaling factor for the plastic model $k_{w,pl}$, the radius of the seal fin r_{sf} and the yield strength at 0.2% offset R_{p02}. If $p_C \leq k_{w,pl}\, R_{p02}$, no plastic wear occurs.

Because wear is a phenomenon on a microscopic scale, the developed equations contain wear parameters which need to be adapted to the experimental results, namely the parameter for abrasive wear $k_{w,a}$, the time constant for the plastic wear t_{pl}, and the parameter for the heat transfer coefficient in the contact area $h_{C,0}$. The data provided by Pychynski [14] shows that these wear parameters also depend on the rubbing scenario. Because experimental data for determining the parameters is not yet available, the values supplied by Pychynski are used. For more information about the applied modelling approach and the validation of the model with experimental results, we refer to Pychynski [14].

Program sequence

In Figure 5, the running sequence of the sub models in the code is illustrated. In order to enable a faster computation, the time scales of the thermal model and the wear processes were separated. The wear time step t_w was reduced in respect to the temperature time step t_T, due to the faster wear processes.
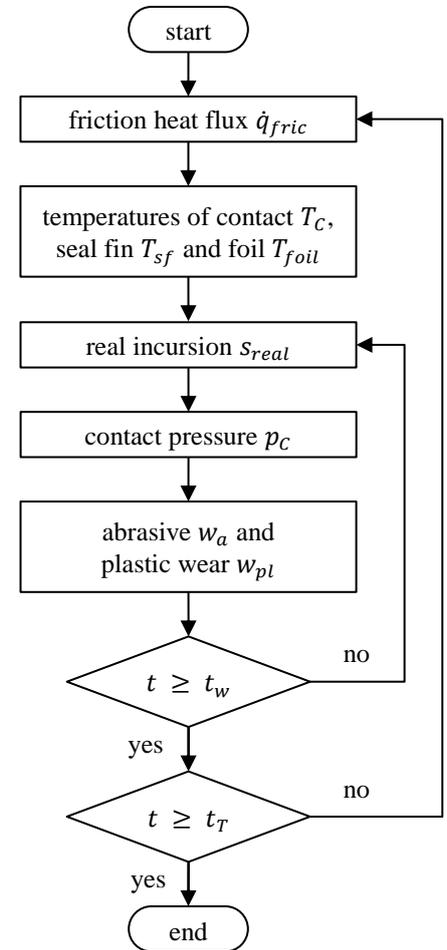

Figure 5 Flow diagram of the program sequence

Material

The rotor material in the present study is Inconel 718, and the metal sheets consist of the nickel-based super-alloys Hastelloy X or Haynes 214. The necessary material properties were taken from data sheets by the manufacturers Haynes International [9, 10] and Special Metals [18]. All material

4

properties are implemented as a function of temperature which are thermal conductivity λ, specific heat c_p, Young's modulus E, yield strength at 0.2% offset R_{p02} and coefficient of thermal expansion α. The results are compared to steel materials stainless austenitic steel X5CrNi18-10 (V2A) for the metal foils and 42CrMo4 (1.7225) for the seal fin.

SYSTEM BEHAVIOUR

Introducing the new material properties into the model, the behaviour and role of the input parameters will change and thus affect the resulting data. Therefore, the results obtained with nickel-based material properties are compared to the results of the steel-steel combination regarding the resulting contact pressure, wear rate, foil temperature at the contact and effective heat partitioning factor. All simulations were performed with the boundary conditions illustrated in Figure 4 and a metal foil thickness of 0.4 mm. The first observation of the system behaviour is that for all investigated rubbing scenarios, the resulting characteristics and quantities for the different stator materials Hastelloy X and Haynes 214 were

similar. Hence, in the following, only the results for Hastelloy X will be discussed.

The results of the simulated contact pressure over the rub velocity for all rub scenarios S1-S5 (see Figure 3) are depicted in Figure 6 a). Additionally, three values of the final incursion depth s_{final} are shown with a second axis on the top. For all rub scenarios, the contact pressure decreases for the nickel-base alloy combination. The contact pressure decreases for increasing final incursion depths because of increasing temperatures in the contact.

The wear of the rubbing system can be described by the resulting wear ratio w_a/w_{tot} at the end of the rubbing process and is shown in Figure 6 b). For the nickel-base alloy combination, the wear ratio decreases in all rub scenarios. That means that the plastic wear has more influence in the rubbing process. This behaviour is attributed to the decreasing contact pressure which leads to decreasing abrasive wear in equation (10). Since the plastic and abrasive wear are in balance, plastic wear must increase.

a) contact pressure

b) wear ratio

c) foil temperature

d) effective heat partitioning factor
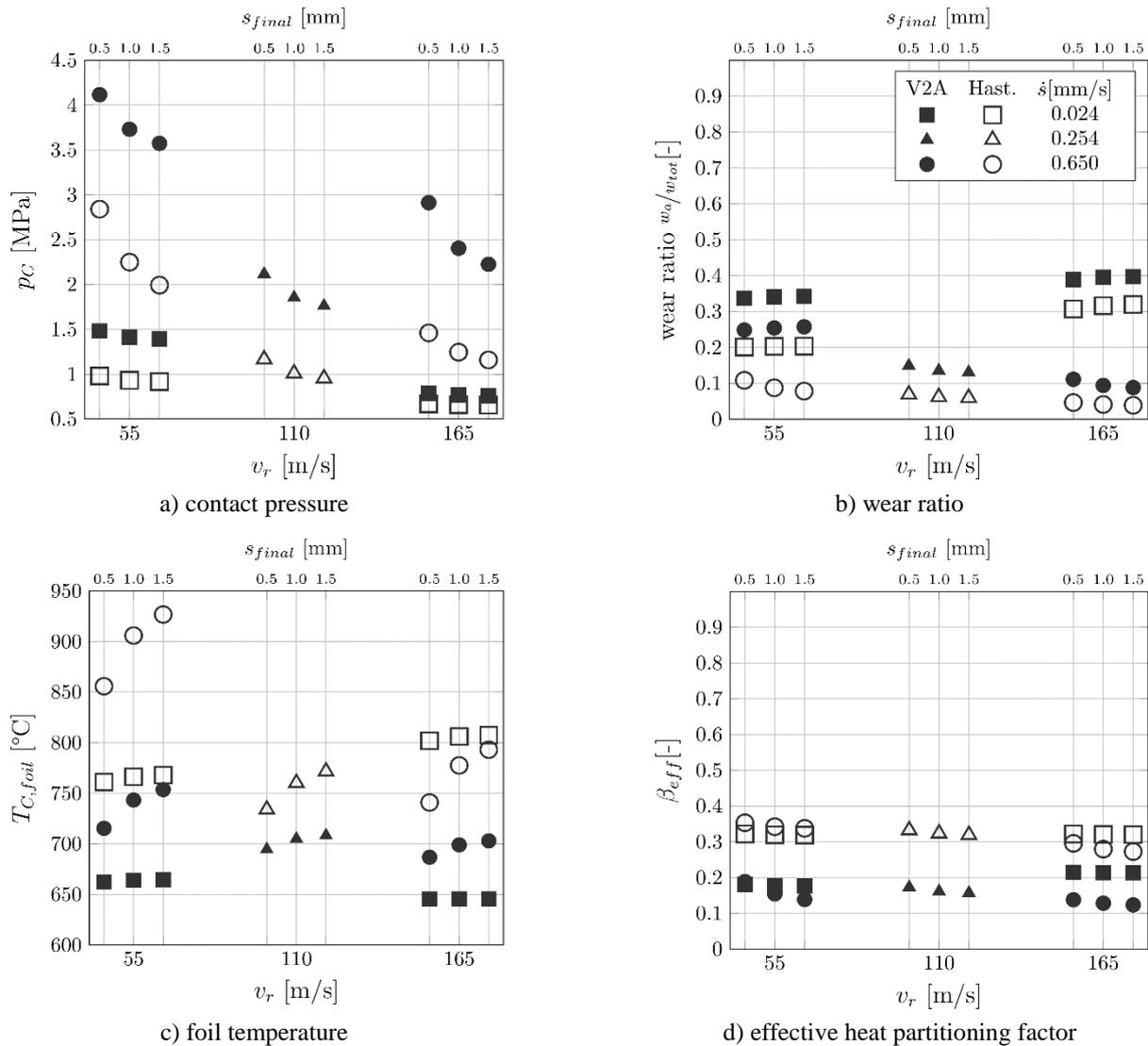
Figure 6 Simulation results for foil width 0.4 mm, the rub scenarios S1-S5, varying incursion rates and material combinations 1.7225/V2A (filled markers), Inconel 718/Hastelloy X (empty markers)

The resulting foil temperature at the contact zone is shown in Figure 6 c). It can be seen that the temperature increases significantly for the nickel-base alloys. The strongest increase can be observed for S1 (high rub velocity, low incursion rate) and S5 (low rub velocity, high incursion rate). Decreasing temperatures for increasing rub velocities were found for the steel model. But in this case, for low incursion rates, the temperature increases with increasing rub velocity. Whereas for high incursion rates, this fact is inverted. Also the proportion of temperatures between the scenarios is inverted. Whereas for low rub velocities, the temperature is higher for high incursion rates, regarding the high rub velocities, the low incursion rate leads to a higher temperature.

Figure 6 d) shows the development of the effective heat partitioning factor. There is a significant increase in the factor for all rub scenarios. As a result, the heat is to a greater extent transported to the metal foil. The qualitative behaviour as a function of the rub velocity is maintained.

The results in the system behaviour are in good agreement with the findings of Pychynski [14]. The higher Young's modulus of the Hastelloy X foil results in an increasing effective heat partitioning factor, which leads to a higher heat flux in the foil resulting in increasing metal foil temperatures. This fact and the increasing Young's modulus in the equation for the heat transfer coefficient (7) and the abrasive wear rate (10) lead to a higher ratio of plastic wear. Therefore, the contact pressure decreases, because the steady state of plastic and abrasive wear is reached sooner due to higher temperatures.

SENSITIVITY STUDY

The presented modelling approach includes several input parameters which are theoretically and experimentally difficult to determine. Therefore, a sensitivity study with the focus on these parameters is carried out. A total of 15 parameters was selected, including mechanical and thermal boundary conditions, tribological model parameters and material properties. The value ranges of the parameters have been set independently of each other by ±25% of the reference values in Table 1. Because the material properties are temperature-dependent, a factor is applied in the complete temperature range. To reduce the correlation between the input parameters, the method of Latin hypercube sampling was used.

For each material combination, a calculation with approximately 32.000 operating points was carried out to make sure that possible interactions between input parameters are assessed. For the analysis, the scenario S3 was used and the metal foil width was set to 0.4 mm. The results obtained for the output parameters contact pressure, wear ratio at the end of the process, effective heat partitioning factor and the temperature in the contact of the seal fin were used for a multi-criteria regression analysis. Since the absolute values of the regression coefficients also depend on the absolute values of the input parameters, the input parameters are normalized to an interval with mean value zero. The resulting linear regression coefficients for the combination of Inconel 718 and Hastelloy X are discussed in the following.

Table 1 Summary of all varied parameters for the sensitivity study [14]

Parameter name	Symbol	Value
Stiffness of the structure	k	350 MPa/mm
Convective heat transfer	h	300 W/m^{2}K
Size of segment	$\varphi_{ec}/2\pi$	15 %
Temperature increase factor of metal foil	$f_{\Delta T,foil}$	0.09
Temperature increase factor of seal fin	$f_{\Delta T,sf}$	1.33
Coefficient of friction	μ	0.156
Heat transfer coefficient	$h_{C,0}$	19000 1/m
Intrinsic heat partitioning factor	β_i	0.5
Abrasive wear coefficient	$k_{w,a}$	22.73
Time constant for plastic wear	t_{pl}	2.5 ms
Factor for thermal conductivity of the metal foil	$f_{\lambda,foil}$	1
Factor for Young's modulus of the metal foil	$f_{E,foil}$	1
Factor for thermal expansion of the metal foil	$f_{\alpha,foil}$	1
Factor for yield strength at 0.2% offset of the metal foil	$f_{Rp02,foil}$	1
Factor for thermal conductivity of the seal fin	$f_{\lambda,sf}$	1

In Figure 7 a), the linear regression coefficients for the contact pressure p_C are shown. A positive coefficient indicates that an increase in the input parameter leads to an increase in the corresponding output parameter. The magnitude provides information about the effect of the input parameter on the output. The order of the bars is according to the influence of the Hastelloy X material combination, leading to the factor with the most influence on the left. The change of material combination has no significant effect on the qualitative influence of the input parameters. The direction of the influence remains unchanged. The main influence on contact pressure is caused by the coefficient of friction μ with $\kappa_{lin}^{pc}(\mu) = -0.60$ and the intrinsic heat partitioning factor β_i with $\kappa_{lin}^{pc}(\beta_i) = -0.56$. Subsidiary influences have the thermal conductivity, $\kappa_{lin}^{pc}(f_{\lambda,foil}) = 0.24$, the heat transfer coefficient, $\kappa_{lin}^{pc}(h_{C,0}) = 0.21$, and Young's modulus, $\kappa_{lin}^{pc}(f_{E,foil}) = -0.20$. With changing the material combination from steel to nickel-base alloys, both the influence of the coefficient of friction μ and the effect of the intrinsic heat partitioning factor β_i increase. The effects of thermal conductivity, heat transfer coefficient and Young's modulus decrease.

The wear ratio depicted in Figure 7 b) is mainly influenced by the Young's modulus of the metal foil, $\kappa_{lin}^{wr}(E_{foil}) = -0.56$, the abrasive wear coefficient, $\kappa_{lin}^{wr}(k_{w,a}) = 0.41$, the coefficient of friction μ, $\kappa_{lin}^{wr}(\mu) = -0.41$ and the intrinsic heat partitioning factor β_i, $\kappa_{lin}^{wr}(\beta_i) = -0.38$. The effect of the thermal conductivity of the metal foil $\kappa_{lin}^{wr}(\lambda_{foil}) = 0.16$ is low and even decreases. Decreasing

contact pressures and increasing Young's modulus with respect to the steel combination leads to a stronger influence of the abrasive wear coefficient $\kappa_{w,a}$ (10).

The strongest effect of the changing material combinations can be observed for the effective heat partitioning factor β_{eff} and the seal fin temperature $T_{C,sf}$. Regarding the partitioning factor in Figure 7 d), the influence of the intrinsic heat partitioning factor increases to $\kappa_{lin}^{\beta}(\beta_i) = 0.84$. The influence of the heat transfer coefficient, $\kappa_{lin}^{\beta}(h_{C,0}) = -0.3$, the Young's modulus, $\kappa_{lin}^{\beta}(E_{foil}) = 0.3$, the thermal conductivity, $\kappa_{lin}^{\beta}(\lambda_{sf}) = -0.22$ and coefficient of friction, $\kappa_{lin}^{\beta}(\mu) = 0.21$ are subsidiary and decrease further with changing material combination to nickel-base alloys. As an effect of the change, the thermal conductivity of the seal fin material significantly decreases. Therefore, the effective thermal conductivity λ_{eff} and the heat transfer in equation (7) decrease. Decreasing heat transfer in the contact reduces the difference between intrinsic and effective heat partitioning. As a result, the influence of the intrinsic heat partitioning increases.

The development of the linear regression coefficients for the seal fin temperature in Figure 7 c) also shows a significant increase in the influence by the intrinsic heat partitioning

factor to $\kappa_{lin}^{Tsf}(\beta_i) = -0.77$. This can also be attributed to the change in thermal conductivity.

CONCLUSIONS

A one-dimensional numerical model was used to describe the system behaviour and perform a sensitivity study of the rubbing process in labyrinth seals for an upcoming experimental investigation. The applied modelling approach is strongly influenced by the adjusted parameters. On one side, this is an indication that the results are of temporary nature and experimental data is needed to produce reliable results. On the other side, the conducted analysis shows that the effect of the adjusted parameters is even increasing. Therefore, the identified main input parameters, which are the intrinsic heat partitioning factor, the coefficient of friction, the Young's modulus of the metal foil and the heat transfer coefficient of the contact need to be the focus of the subsequent experimental investigation.

Nevertheless, the modelling approach under consideration provides a very good opportunity to obtain a deeper physical understanding of the rubbing process. The amount of data produced in a reasonable time frame allows for the investigation of two- and threefold interactions and non-linear effects that are not yet considered in this study.
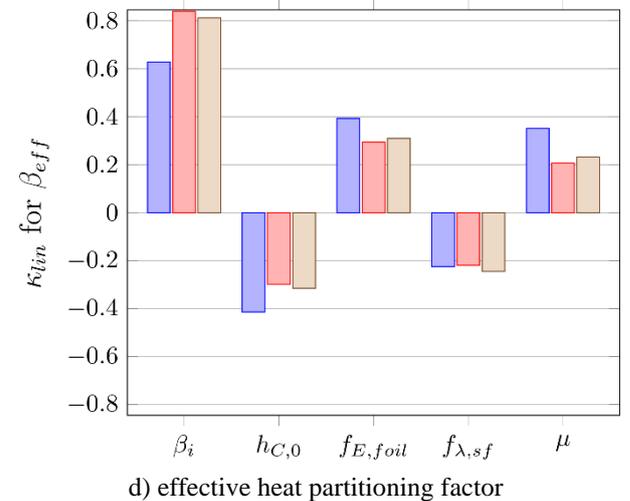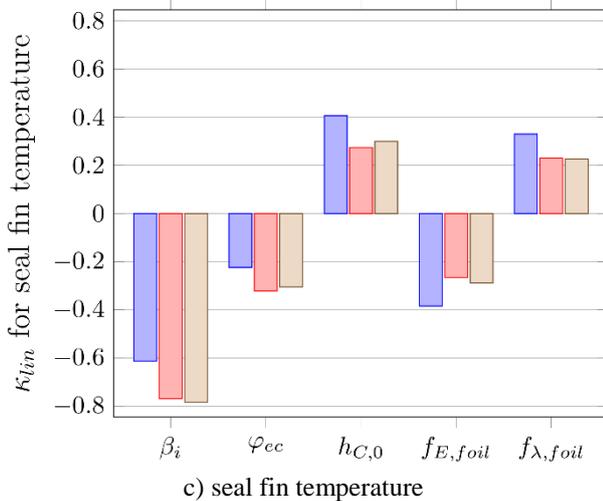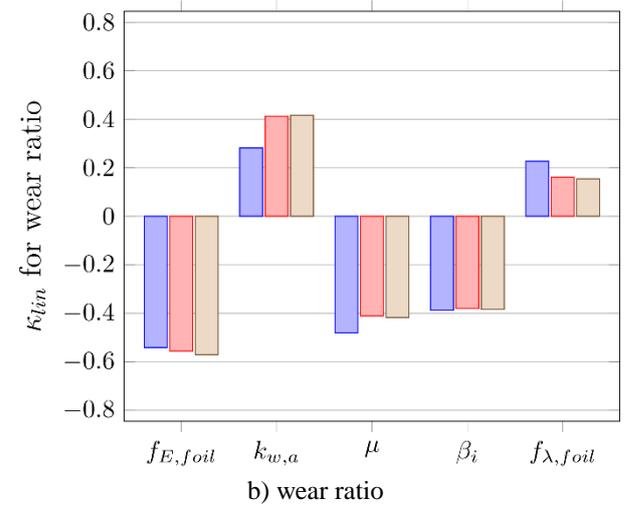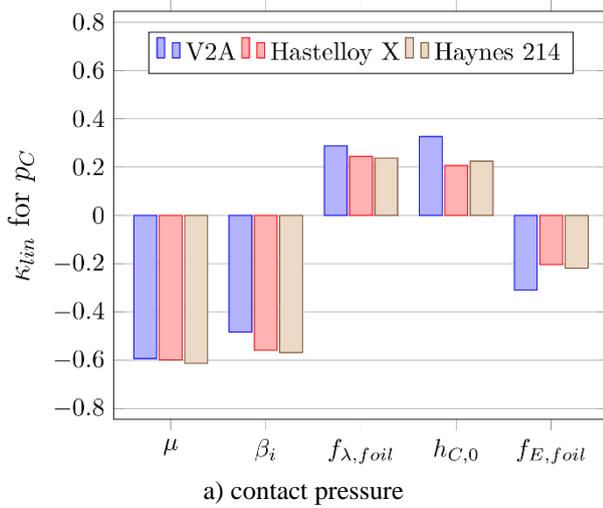

Figure 7 Linear correlation coefficients for the simulation of scenario S3 with a foil thickness of 0.4 mm

NOMENCLATURE

Latin

A	area	[m^2]
B	foil width	[mm]
c_p	specific heat	[J/kg K]
E	Young's modulus	[N/m^2]
f	factor	[-]
F	force	[N]
h	heat transfer coefficient	[W/m^2 K]
$h_{C,0}$	proportionality factor for the heat transfer	[1/m]
k	stiffness coefficient	[N/m^3]
$k_{w,a}$	abrasive wear coefficient	[-]
$k_{w,pl}$	plastic scaling factor	[-]
p	pressure	[MPa]
r	radius	[mm]
R_{p02}	yield strength at 0.2% offset	[N/m^2]
$\dot{q}$	heat flux	[W/m^2]
s	incursion	[mm]
s_{real}	actual incursion	[mm]
t	time	[s]
T	temperature	[K]
v	velocity	[m/s]
w	wear	[m]

Greek

α	thermal expansion	[-]
β	heat partitioning factor	[-]
κ	linear regression coefficient	[-]
μ	coefficient of friction	[-]
λ	thermal conductivity	[W/m K]
φ	angle	[°]

Subscripts

a	abrasive
C	nominal contact area
ec	contact segment
eff	effective
$final$	end of the rubbing process
$foil$	metal foil
$fric$	friction
i	intrinsic
pl	plastic
r	rubbing
sf	seal fin
tot	total

REFERENCES

[1] Archard, J. F. and Hirst, W. 1956. The Wear of Metals under Unlubricated Conditions. *Proceedings of the Royal Society A: Mathematical, Physical and Engineering Sciences* 236, 1206, 397–410.

[2] Bill, R. C. and Ludwig, L. P. 1980. Wear of seal materials used in aircraft propulsion systems. *Wear* 59, 1, 165–189.

[3] Braun, E., Dullenkopf, K., and Bauer, H.-J. Monday 2012. Optimization of Labyrinth Seal Performance Combining Experimental, Numerical and Data Mining Methods. In *ASME Turbo Expo 2012: Turbine Technical Conference and Exposition*, 1847. DOI=10.1115/GT2012-68077.

[4] Chassaing, G., Pougis, A., Philippon, S., Lipinski, P., Faure, L., Meriaux, J., Demmou, K., and Lefebvre, A. 2015. Experimental and numerical study of frictional heating during rapid interactions of a Ti6Al4V tribopair. *Wear* 342-343, 322–333.

[5] Chupp, R. E., Hendricks, R. C., Lattime, S. B., and Steinetz, B. M. 2006. Sealing in Turbomachinery. *Journal of Propulsion and Power* 22, 2, 313–349.

[6] Darecki, M. and others. 2011. Flightpath 2050. Europe's vision for aviation maintaining global leadership & serving society's needs. *Publications Office of the European Union, Luxembourg, Belgium*.

[7] Delebarre, C., Wagner, V., Paris, J. Y., Dessein, G., Denape, J., and Gurt-Santanach, J. 2017. Tribological characterization of a labyrinth-abradable interaction in a turbo engine application. *Wear* 370-371, 29–38.

[8] Ghasripoor, F., Turnquist, N. A., Kowalczyk, M., and Couture, B. 2004. Wear Prediction of Strip Seals Through Conductance. In *ASME Turbo Expo 2004: Power for Land, Sea, and Air*, 331–337. DOI=10.1115/GT2004-53297.

[9] Haynes International, Inc. 1997. *HASTELLOY X Alloy*. High-temperature alloys.

[10] Haynes International, Inc. 2016. *HAYNES 214 Alloy*. High-temperature alloys.

[11] Herrmann, N., Dullenkopf, K., and Bauer, H.-J. Monday 2013. Flexible Seal Strip Design for Advanced Labyrinth Seals in Turbines. In *ASME Turbo Expo 2013: Turbine Technical Conference and Exposition*, V05BT25A035. DOI=10.1115/GT2013-95424.

[12] Ma, H., Yin, F., Guo, Y., Tai, X., and Wen, B. 2016. A review on dynamic characteristics of blade–casing rubbing. *Nonlinear Dyn* 84, 2, 437–472.

[13] Mutasim, Z., Hsu, L., and Wong, E. 1992. Evaluation of plasma sprayed abradable coatings. *Surface and Coatings Technology* 54-55, 39–44.

[14] Pychynski, T. 2016. *Entwicklung und experimentelle Validierung eines Ansatzes für die Modellierung des Anstreifverhaltens von Labyrinthdichtungen mit Honigwabeneinlaufbelägen,* Band 63, ISBN 978-3-8325-4359-4, Logos Verlag.

[15] Pychynski, T., Höfler, C., and Bauer, H.-J. 2016. Experimental Study on the Friction Contact Between a Labyrinth Seal Fin and a Honeycomb Stator. *J. Eng. Gas Turbines Power* 138, 6, 62501.

[16] Rathmann, U., Olmes, S., and Simeon, A. 2007. Sealing Technology: Rub Test Rig for Abrasive/Abradable Systems. In *ASME Turbo Expo 2007: Power for Land, Sea, and Air*, 223–228. DOI=10.1115/GT2007-27724.

[17] Schramm, V., Willenborg, K., Kim, S., and Wittig, S. 2000. Influence of a Honeycomb Facing on the Flow Through a Stepped Labyrinth Seal. In *ASME Turbo Expo 2000: Power*

for Land, Sea, and Air, V003T01A092. DOI=10.1115/2000-GT-0291.

[18] Special Metals Corporation. 2007. *INCONEL alloy 718*.

[19] Zhang, N., Xuan, H.-j., Guo, X.-j., Guan, C.-p., and Hong, W.-r. 2016. Investigation of high-speed rubbing behavior of labyrinth-honeycomb seal for turbine engine application. *J. Zhejiang Univ. Sci. A* 17, 12, 947–960.